ORNL/TM-8256
Dist. Category UC-20 a,f

Contract No. W-7405-eng-26

ORNL/TM--8256

DE82 020477

FUSION ENERGY DIVISION

ELECTRON-CONFINEMENT STUDIES ON EBT-S USING SOFT-X-RAY TECHNIQUES

D. L. Hillis, G. R. Haste, and L. A. Berry

NOTICE This document contains information of a preliminary nature. It is subject to revision or correction and therefore does not represent a final report.

Date Published - August 1982

Prepared by the
OAK RIDGE NATIONAL LABORATORY
Oak Ridge, Tennessee 37830
operated by
UNION CARBIDE CORPORATION
for the
DEPARTMENT OF ENERGY

CONTENTS

ABSTRACT

Soft x-ray bremsstrahlung measurements have been performed on the ELMO Bumpy Torus (EBT-S) plasma to determine the electron temperature T_e and electron density n_e using a calibrated Si(Li) detector over a wide range of operating conditions. The purpose of this paper is to outline the necessary assumptions and essential x-ray techniques that are inherent in soft x-ray measurements in order to investigate the electron heating and confinement properties of EBT-S. In addition, by utilizing the electron density as determined by the soft x-ray measurements, the previous EBT-S confinement analyses have been extended. The steady-state plasma of EBT-S is heated by microwaves using a cw gyrotron that can operate up to power levels of 200 kW. From the soft x-ray measurements, both the electron temperature and density are found to increase at higher microwave power levels. For operation at microwave power levels of 200 kW, T_e approaches 1 keV while n_e approaches 1.2×10^{12} cm^{-3}. In general, confinement properties are found to improve with increased microwave power. The data are compared with neoclasssical transport scaling and the electron transport is found to be collisionless ($\nu/\Omega < 1$) as well as neoclassical.

I. INTRODUCTION

The ELMO Bumpy Torus (EBT)[1,2] is a closed field line device and consists of 24 magnetic mirror cells (2:1 mirror ratio) connected to form a torus with a "bumpy" magnetic field. Plasma production and heating are provided by steady-state microwaves resonant at the electron cyclotron frequency. The plasma of EBT formed via this electron cyclotron resonance heating (ECRH) has two principal plasma components: (1) mirror-trapped high beta, hot electron rings (annuli) and (2) a higher density, lower energy toroidally streaming core plasma. The presence of the high beta, hot electron annulus[3,4] modifies the unfavorable vacuum field and acts to stabilize the toroidally confined core plasma against interchange modes. Also, a cold surface plasma exists near the vacuum vessel walls that is outside the region of closed drift surfaces.

The ECRH power sources in EBT-I ($B_{res} \cong 0.64$ T) utilize klystrons that deliver up to 60 kW for primary heating near the mirror throats and 30 kW of 10.6-GHz microwave power, mainly for profile heating near the outer radial boundary of the plasma. Additional ECRH is available on EBT by using a 28-GHz cw gyrotron that has operated at power levels of up to 200 kW. This upgraded EBT, which is capable of distributing the 200 kW of 28-GHz microwave power and of providing the higher resonant magnetic field ($B_{res} \cong 1$ T), is called EBT-Scale (EBT-S). Typical machine characteristics and physical dimensions for EBT can be found in Refs. 1 and 2.

The overall behavior of the EBT toroidally streaming plasma is characterized by three operating regimes,[5] depending on the microwave power P_μ and the background neutral pressure: (1) The C-mode occurs at

high ambient pressure and/or low microwave power and is characterized by the absence of hot electron rings and by a cold, dense, and noisy plasma; (2) the T-mode occurs at lower pressure when the hot electron rings form and produce a quiescent toroidally confined plasma, which is macrostable; and (3) the M-mode occurs at still lower ambient pressures, where the plasma exhibits MHD type instabilities and the torus begins to appear as disconnected mirror segments.

The purpose of this paper is to utilize soft x-ray techniques in order to investigate the electron heating and confinement properties of EBT-S in the T-mode, where all of the basic EBT concepts are at work. First, questions concerning the validity of using the energy distribution of free-free bremsstrahlung in the soft x-ray regime to determine the toroidally confined electron temperature T_e and density n_e for EBT are addressed. Then, the results from these soft x-ray measurements are used to extend the present understanding of electron heating and confinement on EBT-S. The x-ray analysis system utilizes five calibrated "windowless," lithium-drifted silicon detectors, Si(Li), such that profiles of T_e and n_e can be obtained. In Sec. II the experimental setup used to detect the soft x-ray radiation emitted from EBT-S will be presented and the spectrum analysis techniques employed. In Sec. III, the experimental results are presented for EBT-S as a function of the controllable parameters-microwave power P_μ and ambient pressure p_o. Results from EBT-S operated at continuous wave (cw) microwave powers of 200 kW at 28 GHz indicate that electron temperatures as high as 1 keV and densities of about 1.2×10^{12} cm^{-3} are obtainable. In Sec. IV, the experimental results are compared with neoclassical transport theory.[6-8]

Finally, Sec. V summarizes our conclusions for EBT-S. We conclude that soft x-ray techniques on EBT-S can provide measurements of the electron temperature and density for the toroidally confined plasma. The electron density as measured via the soft x-ray technique is compared with a multichannel microwave interferometer. These two measurements result in the same scaling of the electron density as a function of microwave power; furthermore, the density is found to agree within a factor of 2. We also conclude that even at higher microwave power levels EBT-S continues to support a neoclassical electron confinement model.

II. EXPERIMENTAL DETAILS

A. The detection system

The soft x-ray energy distribution (0.4-6.4 keV) on EBT-S is measured using a vertical array of five lithium-drifted silicon, Si(Li), detectors. The detectors are liquid nitrogen cooled and achieve an energy resolution of ∿180 eV full width half maximum (FWHM). The soft x-ray detection system used on EBT-S is shown in Fig. 1. The array of five Si(Li) detectors is collimated to view the plasma along five parallel chords in the midplane region of one of the EBT cavities. One detector views the central midplane chord, while another views a chord 3.18 cm below the midplane. The remaining three detectors are located vertically above the central chord and separated by 3.18 cm. Incoming x-rays that strike the Si(Li) detector create electron-hole pairs in the crystal in a number proportional to the photon energy E_γ. The resultant pulses are sorted according to their energies and counted by a computer-based pulse height analysis system to yield an x-ray energy spectrum. A typical counting time for collecting an x-ray spectrum is about 300 s; therefore, these measurements represent time-averaged x-ray spectra. Furthermore, using this technique, plasma fluctuations of less than a few hundred milliseconds are not detectable.

Since single photon counting is performed with this technique, great care must be taken to shield against hard x-ray radiation originating from energetic electrons that strike the vacuum vessel of EBT. This is accomplished in part by moving the cavity wall further away from the EBT plasma to form a viewing dump or "black hole" (see Fig. 1). The

entire five-detector assembly is enclosed by ∿5 cm of lead to reduce further the background radiation outside the 15-cm lead enclosure wall. In addition, an elaborate set of lead collimators is used to ensure that each detector sees only a small, well-defined, single chord of the plasma.

Two arrays of filter foils (C, Al, or Be) can be inserted to shield the Si(Li) detectors from ultraviolet or plasma light. Typically, Al foils of ∿90 $\mu g/cm^2$ are used. In order to avoid air attenuation of the soft x-rays the detector is attached to the machine via an evacuated pipe ($\sim 1 \times 10^{-7}$ torr). An ^{55}Fe radioactive source is used to periodically check the detector energy calibration. Due to the microwave environment on EBT a microwave screen is placed between the EBT cavity and the evacuated beamline. This screen consists of numerous closely spaced circular holes, each of which is beyond cut off for the wavelengths used. The transmission efficiency of this screen is about 55% for photons while eliminating microwave leakage from the cavity.

To obtain the maximum soft x-ray efficiency below 1 keV, a "windowless" KEVEX Si(Li) detector is used, i.e., one which does not have a thin beryllium window to maintain the vacuum around the detector. Instead, a gate valve is used in the vacuum line that is opened for data acquisition. Although the elimination of the beryllium window greatly improves the low energy attenuation, other absorbing materials remain. These include a thin, gold electrical contact on the detector face and the silicon dead layer. Special care must be provided for a windowless system due to the LN_2 cooling of the detectors; otherwise, thin layers of condensable gases tend to form on the surface of the detector that

are thick enough to absorb the softest x-rays. To alleviate this problem, a copper, liquid-nitrogen-filled cold finger resides immediately in front of the Si(Li) detectors. Also, an array of thin Al foils ($\sim$90 $\mu g/cm^2$) is placed between the cold finger and the detectors. The combination of these two techniques prevent backstreaming vapors from migrating to the cold detector surfaces.

Due to the possibility of gases freezing out on the cold detector surfaces, the detector efficiency must be checked periodically to ensure that the detector efficiency has not changed. The techniques to determine the absolute detector efficiency on EBT uses an in situ calibration procedure[9] that utilizes the properties of the energetic electron ring. The in situ calibration is determined by operating EBT as a single mirror device. This is accomplished by supplying current to two adjacent coils and microwave power only to the cavity between them. This technique produces a single hot electron ring, without a toroidal plasma component, in the cavity viewed by the soft x-ray detector. The bremsstrahlung spectrum arising from this ring is well represented by a single Maxwellian distribution[10] with $T_e \approx 200$ keV. Thus, a well-defined continuum of x-rays arises from the ring from well below 200 eV up to about 1 MeV. The x-ray energy range of interest for the soft x-ray measurement is $\sim$200 eV to 6 keV. The photon energies produced by the energetic electrons constitute an ideal radiation standard, since no appreciable toroidal plasma is present. First, the x-ray spectrum over the energy range of interest is calculated for a hot electron ring with $T_e \approx 200$ keV. Since the detector efficiency above 3 keV is 100%, the calculation is normalized to the measured spectrum in that region. The

detector efficiency at lower energies can then be determined from the ratio of the observed x-ray spectrum to that calculated for the hot electron ring. The detector efficiency as a function of x-ray energy derived from this technique is shown in Fig. 2. An x-ray source consisting of a hot filament electron source and interchangeable thin foil targets of Al, Cu, and Ti gave efficiencies which were consistent with the hot electron ring techniques.

B. The data analysis method

The x-ray emission from a hydrogenic plasma has been treated extensively in the literature.[11-13] The results for free-free bremsstrahlung will only be summarized here. For a Maxwellian plasma the free-free bremsstrahlung emission is given by

$$\frac{dW}{d\epsilon} = 3.2 \times 10^{-15} n_e \sum_i n_i Z_i^2 T_e^{-1/2} g_{ff}(T_e,\epsilon) e^{-\epsilon/T_e} , \qquad (1)$$

where dW is the power radiated per cubic centimeter per second into the photon energy interval $d\epsilon$; n_e and n_i are the electron and ion density, respectively; Z_i is the ion charge relevant for free-free transitions;[14] g_{ff} is the temperature-averaged gaunt factor[15] for free-free transitions (usually close to 1); and T_e is the electron temperature. From Eq. (1) an enhancement of the bremsstrahlung emission can be produced by impurity ions present in the plasma due to the term $\sum_i n_i Z_i^2$. For EBT-S the dominant impurity ion species are C^{+2}, C^{+3}, Al^{2+}, and Al^{3+} with a few other minor species as determined from spectroscopic measurements.

Typical densities for these ion species are: $n(C^{2+}) \approx 2 \times 10^7$ cm^{-3}, $n(C^{3+}) \approx 6 \times 10^6$ cm^{-3}, $n(Al^{2+}) \approx 6 \times 10^8$ cm^{-3}, and $n(Al^{3+}) \approx 1 \times 10^8$ cm^{-3}. We define Z_{eff} as follows:

$$Z_{eff} \equiv \frac{\sum_i n_i Z_i^2}{n_e}, \tag{2}$$

where the summation is over all ion species. For EBT-S, Z_{eff} is found to be typically 1.007 from spectroscopic measurements, which is an unusually pure hydrogenic plasma.

Another possible contribution to the continuum radiation arises from the process of recombination radiation (free-bound transitions).[12,13] In free-bound scattering, a free electron is captured by an impurity ion, thereby emitting a photon. The photon carries away the kinetic plus the binding energy of the recombining electrons. To illustrate the possible enhancement of the hydrogenic bremsstrahlung spectrum due to recombination radiation from impurity ions, the enhancement factor γ is defined as $\gamma = (dW/d\varepsilon)_{fb}/(dW/d\varepsilon)_{ff}$, following the work of von Goeler.[13] The quantity γ has been evaluated assuming typical densities for Al^{2+} and Al^{3+} under normal EBT-S operating conditions. Throughout the T-mode operating regime the enhancement factor γ was estimated to be about 1.005 to 1.06. This small enhancement for the overall bremsstrahlung spectrum is due to the low charge states and low impurity ion densities observed in EBT. As a result of this small influence of radiative recombination on the overall bremsstrahlung spectrum, it will be ignored in the subsequent analysis.

For typical operating regimes present on EBT-S we are justified in assuming that (1) all electron scattering is due to hydrogen ions ($Z_i^2 \approx 1$), (2) the bulk electron density and ion density are equal ($n_e = n_i$), and (3) $g_{ff} \approx 1.0$. The electron temperature can then be extracted from the measured photon energy distribution by calculating the inverse slope of the data in a semilogarithmic plot of intensity ($dW/d\varepsilon$) versus x-ray energy. The electron density n_e can also be found by solving Eq. (1) for n_e after T_e is determined.

III. EXPERIMENTAL RESULTS

Shown in Fig. 3a is a typical spectrum obtained for an EBT plasma with an applied microwave power P_μ = 150 kW at 28 GHz, a filling pressure of 5.5×10^{-6} torr, and a magnetic field of 0.7 T on axis at the mid-plane of all the EBT cavities. The spectrum has been corrected for foil attenuation, detector efficiency, and count rate. Collection time for this spectrum was 5 min and the fractional solid angle subtended by a single Si(Li) detector is $\Omega/4\pi \cong 2.0 \times 10^{-7}$. The plasma volume viewed by the detector is $\approx$115 cm^3 with an effective chord length of 24 cm assumed for the central plasma diameter. The cavity, where the soft x-ray detection system is located, is not fed directly with microwaves.

Several notable features are present in the spectrum of Fig. 3. Since the soft x-ray detector must view the toroidal core plasma through the hot electron ring plasma, the x-ray spectrum exhibits two distinct x-ray components, namely a high energy x-ray continuum due to the electron rings and a lower energy electron component due to the toroidal core plasma. The most prominent impurity lines are the K_α x-rays from Al (1.5 keV) and the L x-rays (0.93 keV) from Cu. These impurities are the major constituents of the EBT vacuum vessel. The peak occuring at the very lowest energy is due to plasma light and electronic noise.

To illustrate the sensitivity of the soft x-ray detection technique to variations in the toroidal plasma electron temperature and density, two additional soft x-ray spectra are shown in Figs. 3b and 3c. In Fig. 3b, a lower electron temperature and lower density toroidal plasma (T_e = 450 eV and $n_e = 2.5 \times 10^{11}$ cm^{-3}) is produced for EBT-I operation. The spectrum of Fig. 3b resulted from a plasma produced with an applied

microwave power of 40 kW at 18 GHz, a filling pressure of 5.0×10^{-6} torr, and all 24 coils energized to yield $B_{res} = 0.6$ T. Clearly, a smaller number of soft x-rays appear in the lower energy part of the spectrum. Finally, in Fig. 3c a soft x-ray spectrum is displayed for an extremely cold plasma ($T_e < 100$ eV). This is accomplished by using only fundamental resonance heating on EBT.[16] For the measurement of Fig. 3c, EBT was operated with an applied power of 30 kW at 10.6 GHz, a filling pressure of 8.0×10^{-6} torr, and all 24 toroidal field coils energized to $B_{res} \sim 0.38$ T. Figure 3c shows little evidence of a warm toroidal plasma component, which would be superimposed on the hot electron bremsstrahlung component. This is indicative of a very cold ($T_e <$ 100 eV) plasma component and is beyond the capability of the soft x-ray detection system. Even in the presence of the energetic x-rays produced by the hot electron ring, Figs. 3a-c illustrate that significant variations in the toroidal core plasma do occur on EBT and can be detected via the soft x-ray technique.

In order to extract the electron temperature for the toroidal plasma the hard x-ray component arising from the hot electron rings must be subtracted from the spectrum of Fig. 3a. The high energy portion of the spectrum between 4.0 and 6.4 keV is fit by a straight line on a semilog plot (assuming a single Maxwellian hot electron component), and this component is subtracted from the corrected spectrum. The remaining spectrum is due to the toroidal electron component and is shown in Fig. 4. The large aluminum peak has been removed from the spectrum using standard peak fitting techniques to facilitate least squares fitting for determining T_e and n_e. For comparison, a soft

x-ray spectrum from EBT-I is shown in Fig. 4 with P_μ = 40 kW at 18 GHz, a filling pressure of 5.0×10^{-6} torr, and the toroidal field coils energized to produce B_{res} = 0.64 T. The bulk plasma temperature obtained from these data by applying the technique described in Sec. II.B were found to be T_e = 780 eV and $n_e = 0.92 \times 10^{12}$ cm^{-3} for EBT-S and with T_e = 450 eV and $n_e = 2.5 \times 10^{11}$ cm^{-3} for EBT-I.

Following this general analysis procedure T_e and n_e were measured for a variety of different operating conditions on EBT-S. Both the applied microwave power out of the gyrotron P_μ and the ambient gas pressure p_o were varied with soft x-ray spectra being measured at each new condition. The values of T_e for these measurements are shown in Figs. 5 and 6 for the central plasma chord. The corresponding density values are shown in Figs. 7 and 8. Both the electron temperature and density increase as the ambient pressure decreases and/or as the microwave power increases. To further illustrate the microwave power dependence on T_e and n_e, Figs. 9 and 10 show T_e and n_e plotted against P_μ at constant pressure. Both T_e and n_e improve with increased input microwave power.

For the EBT operating conditions that result in rather low values of $T_e \approx 200$ eV (see Figs. 5 and 6), only the high energy tail of the electron distribution can be investigated via the soft x-ray detection method. The practical low energy threshold for x-ray detection with the present system is about 400 eV. For the lowest electron temperatures on EBT ($\sim$200 eV), only about 25% of the electrons contribute to the observed x-ray spectrum. On the other hand, for electron temperatures that are greater than 600 eV, more than 75% of the x-ray energy distribution is

being examined. For these higher electron temperatures, it is less likely that a high energy electron tail is involved in producing the observed soft x-ray spectra. Also, due to the line-averaged nature of the soft x-ray measurements, there is a basic insensitivity to hollow profiles.

The purpose of the multichannel five-detector Si(Li) array is to provide profile information about $T_e(r)$ and $n_e(r)$, where r is the chord location as measured radially outward from the center of the EBT-S cavity. Figures 11 and 12 show radial profiles of T_e and n_e for several 28-GHz microwave power levels as well as an EBT-I case with 40 kW at 18-GHz microwave power. The individual chord-averaged values of $n_e(r)$ are derived by assuming that the plasma being viewed is bounded by the hot electron ring. The profile measurements of T_e and n_e are shown as ratios, $T_e/T_e(0)$ and $n_e/n_e(0)$, where $T_e(0)$ and $n_e(0)$ are the values measured for the central chord. The ring location is indicated via the cross-hatched region at $r \approx 12$ cm. Within the error bars, the profiles for both T_e and n_e are reasonably flat over the 10-cm range for all values of microwave power. The flatness of these profile measurements is in agreement with both Thomson scattering[17] results and results from a multichannel microwave interferometer.[18]

The electron density on EBT-S is also measured with a nine-channel microwave interferometer.[17] These multichannel interferometer data are Abel inverted and provide the central or peak electron density at the plasma center. Shown in Fig. 13 is a comparison of the electron densities determined via soft x-ray measurements and the nine-channel microwave interferometer for various 28-GHz microwave power levels. Data for two

separate torus filling pressures are shown. It should be noted that n_e as measured with the interferometer corresponds to a central density at the plasma center, whereas n_e as measured with the soft x-ray diagnostic corresponds to a line-averaged electron density. Typically, the electron density as measured by the microwave interferometer is approximately 1.4-1.8 times the line averaged electron density as measured by soft x-ray techniques. These differences are most likely due to uncertainties in the Abel inversion process when contributions to n_e are included for the cold surface plasma. The soft x-ray technique is insensitive to the colder surface plasma, which would produce x-rays below 400 eV in energy. Even though the absolute values of the electron densities as determined by soft x-ray and by microwave interferometry are not in exact agreement, the two techniques do produce the same scaling of the electron density with microwave power. Therefore, for the scaling studies presented herein, the results are unaffected by whether the microwave interferometer or the soft x-ray electron density is used. For the scaling studies presented in Sec. IV, the soft x-ray density n_e will be used since a larger set exists for these measurements.

IV. CONFINEMENT STUDY OF THE TOROIDAL PLASMA

Radial transport in bumpy tori has been investigated by several authors.[6-8] Neoclassical theory was applied by Kovrizhnykh[8] to compute analytic expressions for particle and energy fluxes across magnetic fields in various toroidal magnetic systems. For bumpy tori, Kovrizhnykh considered only the limit of very large radial electric fields where the results do not depend on the poloidal component of the electric field. More recently, Jaeger et al.[6] have calculated these neoclassical transport coefficients for EBT for an arbitrary electric field and have applied these coefficients in a one-dimensional (1-D) radial transport model that includes the ambipolar field self-consistently.

In the absence of losses induced by instabilities, the dominant loss mechanisms of the toroidal core electrons in EBT-S are diffusive. The energy balance equation then becomes

$$\alpha P_{\mu} = \frac{3/2 n_e T_e V_p}{\tau_E} , \tag{3}$$

where αP_{μ} is the amount of microwave power that heats the core electrons in EBT at the electron cyclotron frequency, α is the fraction of microwave power absorbed by the core plasma and taken to be 12% (discussed later), τ_E is the electron energy confinement time, and V_p is the total toroidal core plasma volume, which is 0.3 m^3.

The basis for neoclassical transport[8,19-20] in EBT is that the diffusion coefficients, such as electron thermal conductivity, depend on a step size Δx, which scales as

$$(\Delta x)^2 = (V_T/\Omega)^2 \left(\frac{\Omega^2}{\nu^2 + \Omega^2}\right) , \tag{4}$$

where V_T is the vertical drift produced by toroidal curvature, ν is the electron collision frequency, and Ω is the poloidal drift frequency produced by the bumpy magnetic field. The factor $\Omega^2/(\nu^2 + \Omega^2)$ is included to take into account the more collisional regimes where particles are unable to complete their poloidal drift about the axis in time ν^{-1}. That is,

$$V_T = T/(eBR) \tag{5}$$

and

$$\Omega = \Omega_{\nabla B} + \Omega_{E\times B} = \frac{T_e}{eBrR_c}\left(1 + \gamma \frac{e\phi}{T_e}\right) , \tag{6}$$

where $\gamma = 2rR_c/a^2$, B is the magnetic field, R is the major radius of EBT, r is the minor radius, ϕ is the ambipolar potential, a is the plasma radius, and $R_c = (-\nabla B/B)^{-1}$ is the average scale length in the bumpy magnetic field. Combining Eq. (4) with $D = \Delta x^2 \nu$ we arrive at the diffusion coefficient for electrons

$$D \sim \left(\frac{V_T^2}{\Omega}\right)^2 \frac{\Omega^2}{\nu^2 + \Omega^2} \nu . \tag{7}$$

This simplified heuristic description gives the result found by Kovrizhnikh[8] for describing nonaxissymmetric systems. Two limits of

collisionality are easily identified: $\nu >> \Omega$ (the collisional regime, $\nu/\Omega > 1$) and $\nu << \Omega$ (the collisionless regime, $\nu/\Omega < 1$). Equation (7) in these two limits reduces to

$$D = \frac{(V_T)^2}{\nu} \qquad \nu >> \Omega \tag{8}$$

and

$$D = \left(\frac{V_T}{\Omega}\right)^2 \nu \qquad \nu << \Omega \ . \tag{9}$$

More detailed kinematic calculations of the transport coefficients have been completed by Spong et al.[19] These calculations include most of the principal mechanisms that affect electron transport. Even with the more refined analyses[6,7,21-25] the functional of Eq. (7) survives as part of all transport coefficients.

The collisionality $(\nu/\Omega)_e$ for electrons is given as

$$\left(\frac{\nu}{\Omega}\right)_e = C_o B r R_c \frac{n_e}{T_e^{5/2}} \left(1 + \gamma \frac{e\phi}{T_e}\right) \ , \tag{10}$$

where C_o is the coefficient in the electron collision frequency

$$\nu_e = C_o \frac{n_e}{T_e^{3/2}} \ . \tag{11}$$

Using Eq. (10) the collisionality $(\nu/\Omega)_e$ has been evaluated using the experimental values of n_e and T_e for EBT-S. The value of $e\phi/T_e$ was also

measured and found, over the parameter range studied, to be ≈ 0.6.[18] Figure 14 shows the collisionality plotted as a function of ambient pressure at various input microwave power levels. For the entire pressure and microwave power range studied, $(\nu/\Omega)_e$ is less than one and clearly shows that EBT operates in the collisionless regime. Furthermore, for a constant ambient pressure, $(\nu/\Omega)_e$ decreases with increasing microwave power. Some stable regions at higher values of ν/Ω have been observed experimentally, but the electron temperatures under these conditions are lower and outside the range of measurability using bremsstrahlung as a diagnostic tool.

For a macrostable plasma, EBT-S is normally operated in the collisionless regime ($\nu/\Omega < 1$) and the diffusion coefficient is given by Eq. (7). Combining Eqs. (5), (6), (9), and (11) yields

$$D \sim \frac{n_e}{T_e^{3/2}} r^2 \left(\frac{R_c}{R}\right)^2 . \tag{12}$$

Since $1/\tau_E \sim D/a^2$ we can estimate the energy confinement time for EBT:

$$\tau_E \sim \frac{T_e^{3/2}}{n_e} \left(\frac{a}{r}\right)^2 \left(\frac{R}{R_c}\right)^2 . \tag{13}$$

For EBT-S, $a/r \sim 1$ and $R/R_c \sim A$, the magnetic aspect ratio. The magnetic aspect ratio for EBT is $A >> 1$. Thus, we obtain for EBT

$$n\tau_E \sim A^2 \, T_e^{3/2} . \tag{14}$$

To estimate τ_E from the experimental measurements of n_e and T_e, the energy balance Eq. (3) can be used, providing the value of αP_μ is known. Experimentally, this is difficult because the amount of microwave power αP_μ to sustain the toroidal plasma is not directly measurable. Rather, it is necessary to determine the amount of power required to sustain each plasma component. If the ring power P_R, the surface plasma power P_s, and the power lost P_L to cavity walls and waveguides are separately measured and subtracted from the total power P_μ out of the gyrotron, it is possible to estimate the power required to sustain the toroidal plasma, αP_μ:

$$\alpha P_\mu = P_\mu - P_L - P_R - P_S \ , \tag{15}$$

where $P_L \approx 0.33P_\mu$, $P_R \approx 0.10P_\mu$, and $P_S \approx 0.45P_\mu$. This division of microwave power indicates that ~12% of the applied microwave power is effective in heating the toroidal plasma. A theoretical justification for this division of microwave power can be found also in Ref. 26.

Utilizing Eq. (3) with $\alpha = 12\%$, τ_E was calculated. Figure 15 shows τ_E plotted as a function of ambient pressure for several values of P_μ. Clearly, τ_E improves with increasing levels of applied microwave power. These same trends were found by Jaeger et al.[7] for the collisionless regime.

To illustrate the agreement with our simple neoclassical scaling argument presented in Eq. (14), the values of $n\tau_E$ are plotted against T_e in Fig. 16. The data are then compared with the expected $n\tau_E \sim T_e^{3/2}$ scaling. The agreement is remarkable and supports neoclassical scaling for EBT-S.

A second neoclassical scaling can be obtained by combining Eqs. (3) and (14) to get

$$T_e(\alpha P_\mu)^2 \sim n^4 \ . \tag{16}$$

The data are plotted in this fashion in Fig. 17 and compared with the predicted behavior of Eq. (16). Again, the data are in excellent agreement with the expected neoclassical prediction.

The neoclassical scaling of EBT has also been presented in the work of Ref. 18. In this work, the line-averaged electron density $n_e\ell$, as determined by a microwave interferometer, was used. They found it necessary in their analysis to hold the density profiles constant. Under these conditions, they were able to illustrate the neoclassical scaling of EBT. On the other hand, our soft x-ray measurements are sensitive only to the hot electron population and are probably less influenced by the cold surface plasma (as compared with the interferometer density used in Ref. 18). We therefore did not find it necessary to invoke the constraint that density profiles remain constant to illustrate the neoclassical behavior of EBT.

Finally, to indicate that particle and energy confinement improve with increased microwave power, we plot n_eT_e as a function of the ratio P_μ/p_o. Since $\tau_E \sim n_eT_e/P_\mu$ and

$$\tau_p = \frac{1}{n_o\langle\sigma v\rangle_i} \sim \frac{1}{p_o} \ , \tag{17}$$

then

$$n_eT_e \sim \left(\frac{\tau_E}{\tau_p}\right)\frac{P_\mu}{p_o} \ , \tag{18}$$

where p_o is the ambient pressure, n_o is the neutral density, and $\langle \sigma v \rangle_i$ is the ionization rate coefficient. The slope of the curve in Fig. 18 is therefore indicative of the ratio (τ_E/τ_p). It is encouraging that the ratio τ_E/τ_p increases with increasing P_μ or with decreasing pressure.

V. SUMMARY

Soft x-ray measurements have been performed to determine the plasma electron temperature and electron density for EBT-S using a calibrated Si(Li) detector over a wide range of operating conditions. The experiments have demonstrated the validity of the concept of macroscopically stable confinement of a warm toroidal plasma in a bumpy torus, which is stabilized by diamagnetic annuli. From the soft x-ray measurements the following conclusions can be made:

(1) Both the electron temperature and the electron density increase with increasing microwave power and/or decreasing ambient pressure.

(2) The energy confinement time τ_E improves with increased microwave power or decreased ambient pressure.

(3) The electron temperature and density profiles were found to be flat or only gently varying over the radial extent of the plasma out to the location of the hot electron ring.

(4) The electron transport in EBT-S is found to be collisionless ($\nu/\Omega << 1$) as well as neoclassical.

ACKNOWLEDGMENTS

The authors would like to express their appreciation to C. L. Hedrick, E. F. Jaeger, and the members of the EBT experimental group for their valuable input and suggestions to this manuscript. The assistance of the EBT operations group is also gratefully acknowledged.

REFERENCES

1. R. A. Dandl et al., ORNL/TM-3694, 1971; R. A. Dandl et al., in *Plasma Physics and Controlled Nuclear Fusion Research 1974*, Vol. II (IAEA, Vienna, 1975), p. 141.
2. J. C. Glowienka, J. Vac. Sci. Technol. 18(3), 1088 (1981).
3. R. A. Dandl et al., in *Plasma Physics and Controlled Nuclear Fusion Research 1968*, Vol. II (IAEA, Vienna, 1975), p. 435; R. A. Dandl et al., in *Plasma Physics and Controlled Nuclear Fusion Research 1971*, Vol. II (IAEA, Vienna, 1972), p. 607.
4. N. A. Uckan, ed., *EBT Ring Physics, Proceedings of Workshop*, CONF-791228 (Oak Ridge, Tennessee, 1979).
5. R. A. Dandl et al., in *Plasma Physics and Controlled Nuclear Fusion Research*, Vol. II (IAEA, Vienna, 1979), p. 365; Oak Ridge National Laboratory Reports ORNL/TM-4941, 1975, and ORNL/TM-6457, 1978.
6. E. F. Jaeger, D. A. Spong, and C. L. Hedrick, Phys. Rev. Lett. 40, 866 (1978).
7. E. F. Jaeger, C. L. Hedrick, and W. B. Ard, Phys. Rev. Lett. 43, 855 (1979).
8. L. M. Kovrizhnykh, Sov. Phys.-JETP 29, 475 (1969).
9. S. Hiroe, G. R. Haste, and R. A. Dandl, ORNL/TM-6820, 1979.
10. N. A. Uckan et al., in *Plasma Physics and Controlled Nuclear Fusion Research 1980*, Vol. I (IAEA, Vienna, 1981), p. 831; D. L. Hillis, Oak Ridge National Laboratory Report ORNL/TM-8179 (1982).
11. S. von Goeler et al., Nucl. Fusion 15, 301 (1975).
12. T. F. Stratton, *Plasma Diagnostic Techniques* (Academic Press, New York, 1965), p. 362.

13. S. von Goeler, *Diagnostics for Fusion Experiments* edited by E. Sindoni and C. Wharton (Pergamon Press, Oxford and New York, 1979), p. 79.

14. S. von Goeler, W. Stodiek, H. Eubank, H. Fishman, S. Grebenshchikov, and H. Hinnov, Nucl. Fusion 15, 301 (1975).

15. W. J. Karzas and R. Latter, Astrophys. J. Suppl. 55, 167 (1961).

16. J. C. Glowienka, W. A. Davis, D. L. Hillis, T. Uckan, F. M. Bieniosek, and L. Solensten, Oak Ridge National Laboratory Report ORNL/TM-8180 (1982).

17. L. Bighel and J. A. Cobble, Phys. Rev. Lett. 46, 430 (1981) and Oak Ridge National Laboratory Report ORNL/TM-7437 (1980).

18. T. Uckan, L. A. Berry, D. L. Hillis, and R. K. Richards, ORNL/TM-8117 (1981), to be published in Phys. Fluids.

19. D. A. Spong et al., Nucl. Fusion 19, 665 (1979).

20. M. Fujiwara et al. (NBT) group and F. W. Baity et al. (EBT group), in *Plasma Physics and Controlled Nuclear Fusion Research 1980*, Vol. I (IAEA, Vienna, 1981), p. 845.

21. D. A. Spong and C. L. Hedrick, Phys. Fluids 24, 290 (1981).

22. R. D. Hazeltine and P. J. Catto, Phys. Fluids 24, 290 (1981).

23. E. F. Jaeger and C. L. Hedrick, Nucl. Fusion 19, 433 (1979).

24. E. F. Jaeger, C. L. Hedrick, and D. A. Spong, Nucl. Fusion 19, 1627 (1979).

25. E. F. Jaeger et al., Oak Ridge National Laboratory Report ORNL/TM-7558 (1980).

26. D. B. Batchelor, Oak Ridge National Laboratory Report ORNL/TM-7001 (1981).

FIGURE CAPTIONS

FIG. 1. Windowless Si(Li) detection system used on EBT for soft x-ray measurements.

FIG. 2. Si(Li) detector calibration which shows measurements of the detector efficiency vs x-ray energy (see text).

FIG. 3. Typical soft x-ray bremsstrahlung spectra observed during EBT operation with single frequency microwave heating: (a) A typical soft x-ray spectrum during EBT operation with 150 kW of 28-GHz microwave power with an ambient pressure of 5.5×10^{-6} torr. (b) and (c) Spectra observed using the 18-GHz and 10.6-GHz microwave sources, respectively. The spectra are characterized by a high energy continuum of x-rays due to the energetic electron rings and a lower energy soft x-ray component (<2 keV) due to the toroidally streaming bulk plasma. (Further details are in the text.)

FIG. 4. Soft x-ray component due to the toroidally streaming bulk plasma after subtraction of energetic x-rays due to the hot electron ring. The solid lines represent the best fit to the data with the values of T_e and n_e as indicated. For comparison, results from EBT-I and EBT-S are shown.

FIG. 5. The electron temperature obtained for EBT-S using the soft x-ray detection system is plotted against ambient pressure at four values of microwave power (50, 100, 150, and 200 kW). The data shown are for single frequency microwave heating with the 28-GHz gyrotron alone.

FIG. 6. The electron temperature obtained for EBT-S using the soft x-ray detection system is plotted against ambient pressure at four values of microwave power (25, 75, 125, and 175 kW). The data shown are for single-frequency microwave heating with the 28-GHz gyrotron.

FIG. 7. The electron density obtained for EBT-S using the soft x-ray detection system is plotted against ambient pressure at four values of microwave power (50, 100, 150, and 200 kW). The data shown are for single-frequency microwave heating using the 28-GHz gyrotron.

FIG. 8. The electron density obtained for EBT-S using the soft x-ray detection system is plotted against ambient pressure at four values of microwave power (25, 75, 125, and 175 kW). The data shown are for single-frequency microwave heating using the 28-GHz gyrotron.

FIG. 9. The electron temperature, as measured by the soft x-ray detection system, is plotted against microwave power out of the 28-GHz gyrotron for several values of ambient pressure (5×10^{-6}, 6×10^{-6}, 7×10^{-6}, and 10×10^{-6} torr).

FIG. 10. The electron density, as measured by the soft x-ray detection system, is plotted against microwave power out of the 28-GHz gyrotron for several values of ambient pressure (5×10^{-6}, 6×10^{-6}, 7×10^{-6}, and 10×10^{-6} torr).

FIG. 11. Electron temperature profiles as measured by the five-channel soft x-ray detection system. The value $T_e/T_e(0)$ is the ratio of the electron temperature at location r divided by the electron temperature at r = 0 cm. The cross-hatched region indicates the location of the hot electron ring. The operating parameters of EBT are also shown for each measurement.

FIG. 12. Electron density profiles as measured by the five-channel soft x-ray detection system. The value $n_e/n_e(0)$ is the ratio of the electron density at location r divided by the electron temperature at r = 0 cm. The cross-hatched region indicates the location of the hot electron ring in each measurement. The operating parameters of EBT are also shown for each measurement.

FIG. 13. The electron density n_e as measured with a multichannel microwave interferometer is compared with that found using the soft x-ray technique. The density is plotted for both diagnostics as a function of applied microwave power for two separate torus filling pressures. (See text for discussion.)

FIG. 14. Collisionality is plotted against ambient pressure with microwave power as a parameter. Typical error bars are also shown for a few data points.

FIG. 15. The energy confinement time τ_E is calculated from the soft x-ray results and is plotted as a function of ambient pressure at four values of applied microwave power at 28 GHz. It is encouraging that τ_E improves as the microwave power levels are increased. (See text for further discussion.)

FIG. 16. The quantity $n_e\tau_E$, which is derived from the soft x-ray results is plotted as a function of the electron temperature T_e. Data are presented for applied microwave power levels of 50, 100, 150, and 200 kW. The solid line compares the theoretical neoclassical dependence $n\tau_E \propto T_e^{3/2}$ with the data. Clearly, EBT appears to scale neoclassically.

FIG. 17. The quantity $T_e(\alpha P_\mu)^2$, which is derived from the soft x-ray results, is plotted as a function of the electron density n_e. Data are presented for applied microwave power levels of 50, 100, 150, and 200 kW. The solid line compares the theoretical neoclassical dependence $T_e(\alpha P_\mu)^2 \propto n_e^4$ with the data. Typical error bars are indicated for the data.

FIG. 18. Energy density of the bulk plasma, $n_e T_e$, is plotted against the value P_μ/p_o. Typical error bars are indicated. The slope of this data plot is proportional to τ_E/τ_p. (See text for explanation.)

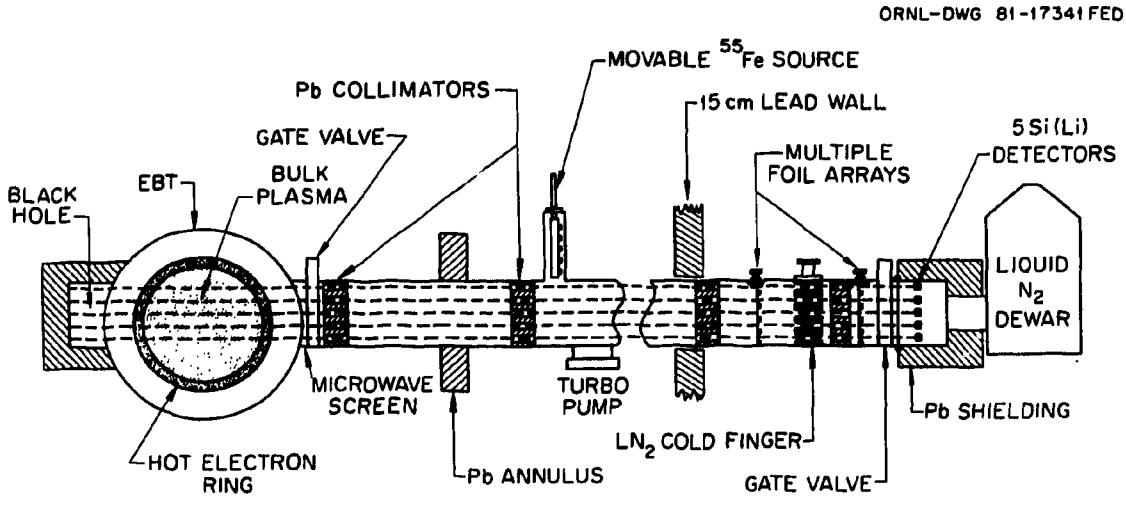
ORNL-DWG 81-17341 FED
MOVABLE ^{55}Fe SOURCE
Pb COLLIMATORS
15 cm LEAD WALL
5 Si(Li) DETECTORS
GATE VALVE
MULTIPLE FOIL ARRAYS
BLACK HOLE
EBT
BULK PLASMA
LIQUID N_2 DEWAR
MICROWAVE SCREEN
TURBO PUMP
Pb SHIELDING
LN_2 COLD FINGER
HOT ELECTRON RING
Pb ANNULUS
GATE VALVE

Fig. 1

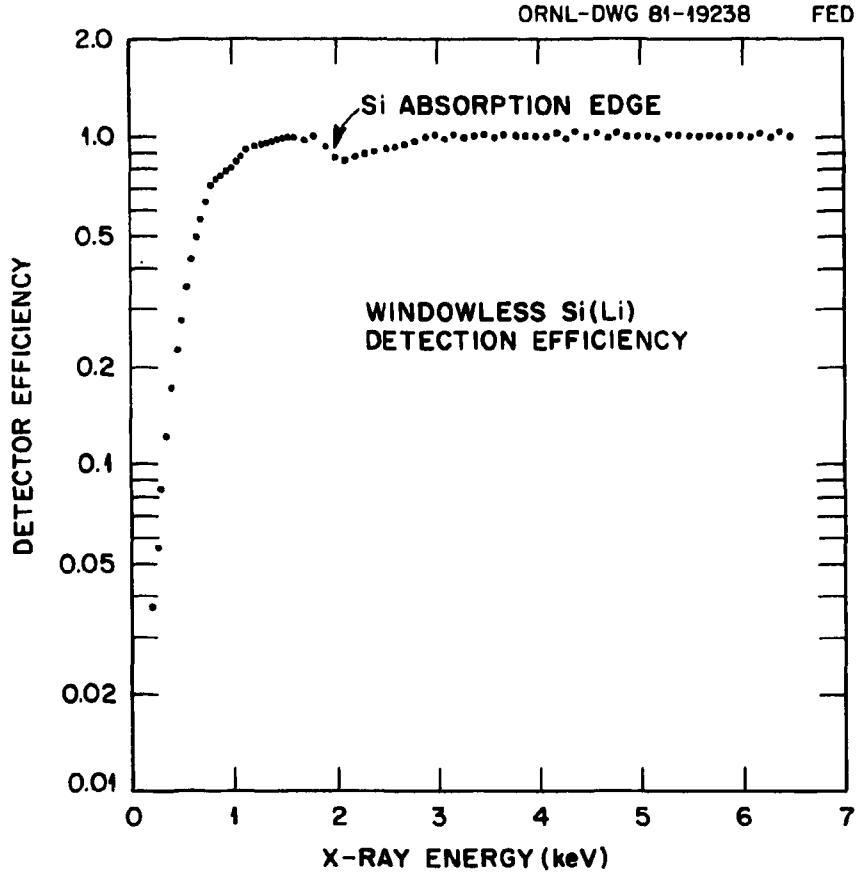
ORNL-DWG 81-19238 FED
Si ABSORPTION EDGE
WINDOWLESS Si(Li)
DETECTION EFFICIENCY
DETECTOR EFFICIENCY
2.0
1.0
0.5
0.2
0.1
0.05
0.02
0.01
0
1
2
3
4
5
6
7
X-RAY ENERGY (keV)

Fig. 2

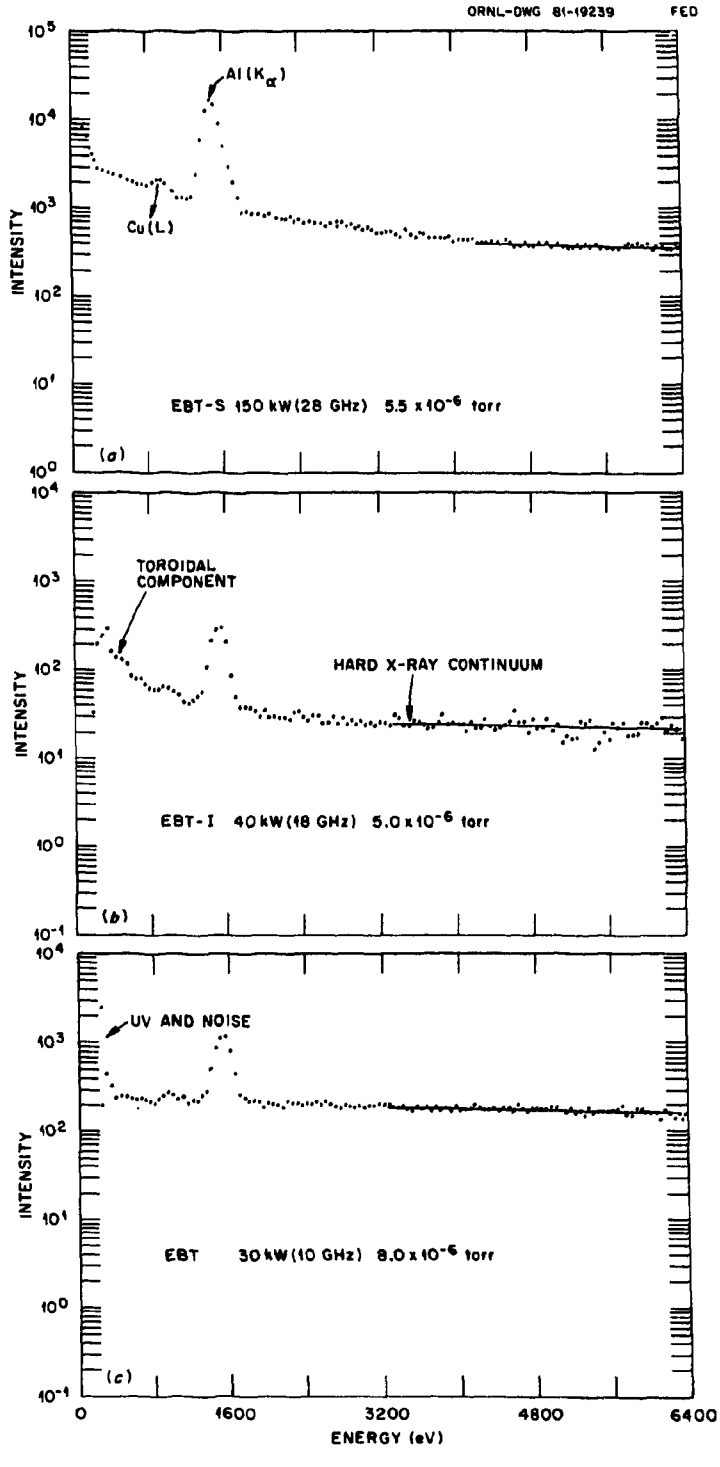
ORNL-DWG 81-19239 FED
Al(K_α)
Cu(L)
EBT-S 150 kW(28 GHz) 5.5 x10^{-6} torr
(a)
TOROIDAL COMPONENT
HARD X-RAY CONTINUUM
EBT-I 40 kW(18 GHz) 5.0 x10^{-6} torr
(b)
UV AND NOISE
EBT 30 kW(10 GHz) 8.0 x10^{-6} torr
(c)
INTENSITY
0
1600
3200
4800
6400
ENERGY (eV)

Fig. 3

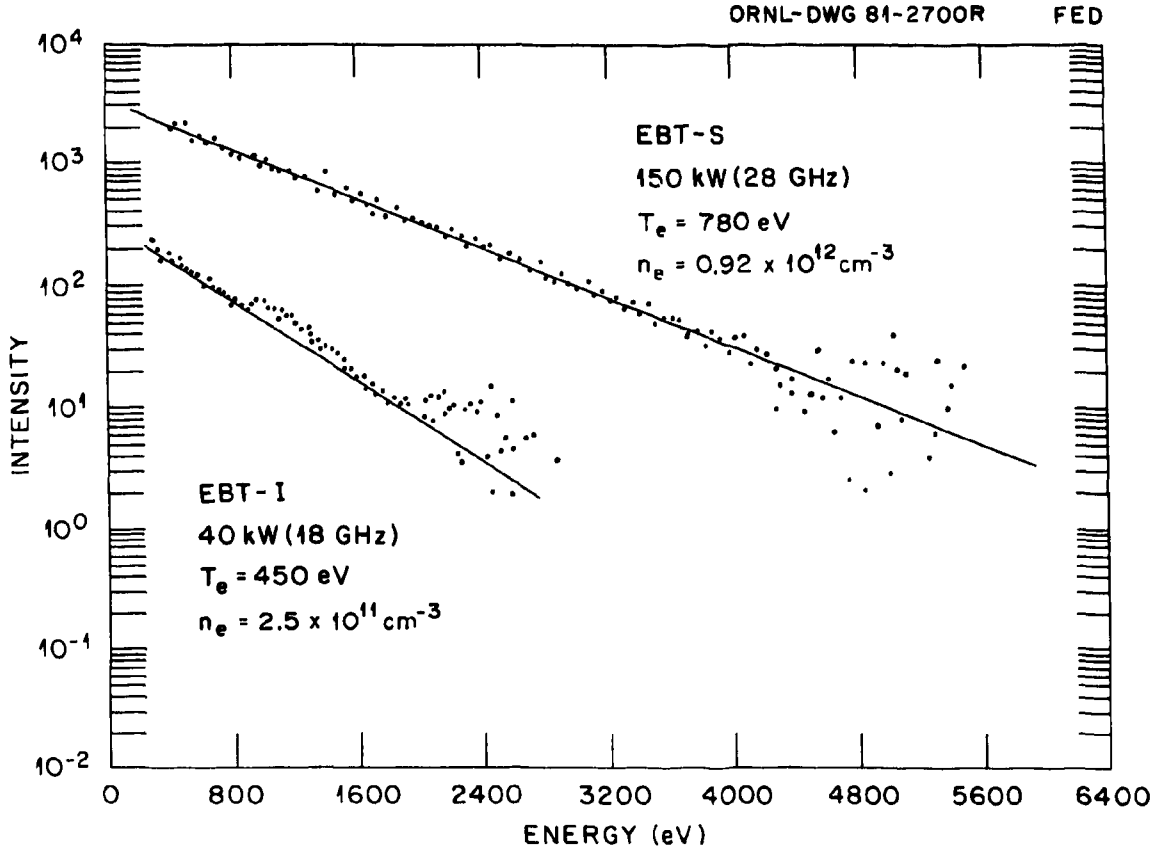
ORNL-DWG 81-2700R FED
EBT-S
150 kW (28 GHz)
T_e = 780 eV
n_e = 0.92 x 10^{12} cm^{-3}
EBT-I
40 kW (18 GHz)
T_e = 450 eV
n_e = 2.5 x 10^{11} cm^{-3}
INTENSITY
10^4
10^3
10^2
10^1
10^0
10^{-1}
10^{-2}
0
800
1600
2400
3200
4000
4800
5600
6400
ENERGY (eV)

Fig. 4

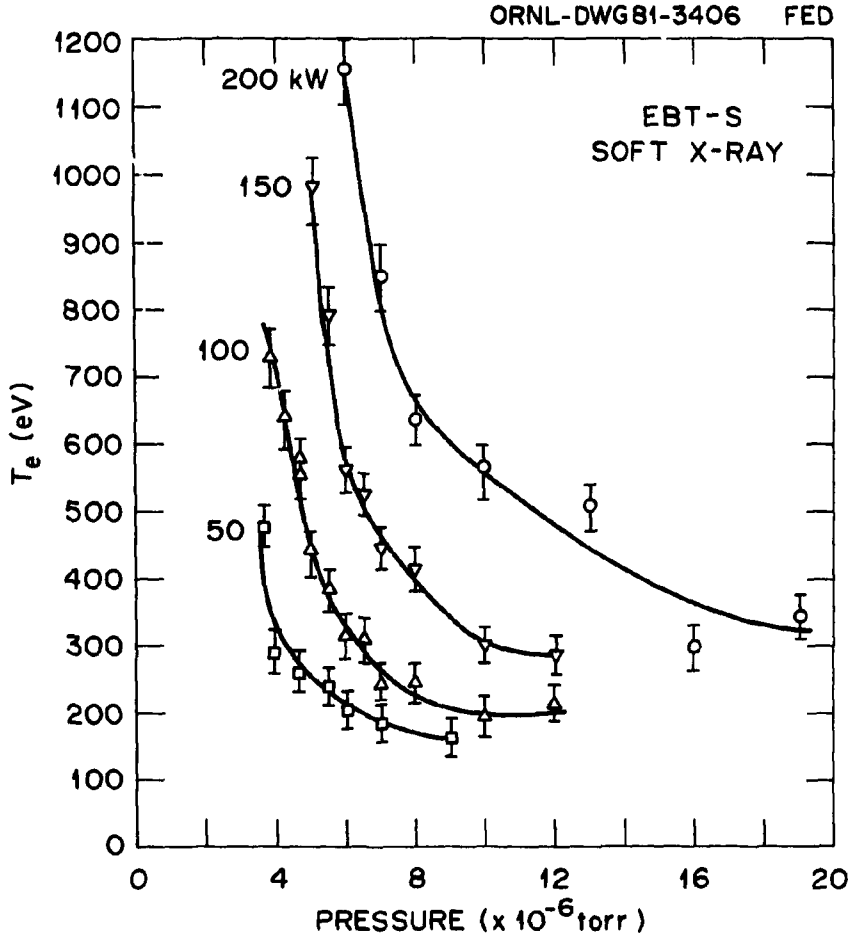
ORNL-DWG81-3406 FED
EBT-S
SOFT X-RAY
200 kW
150
100
50
T_e (eV)
PRESSURE (x 10^{-6} torr)
0
100
200
300
400
500
600
700
800
900
1000
1100
1200
0
4
8
12
16
20

Fig. 5

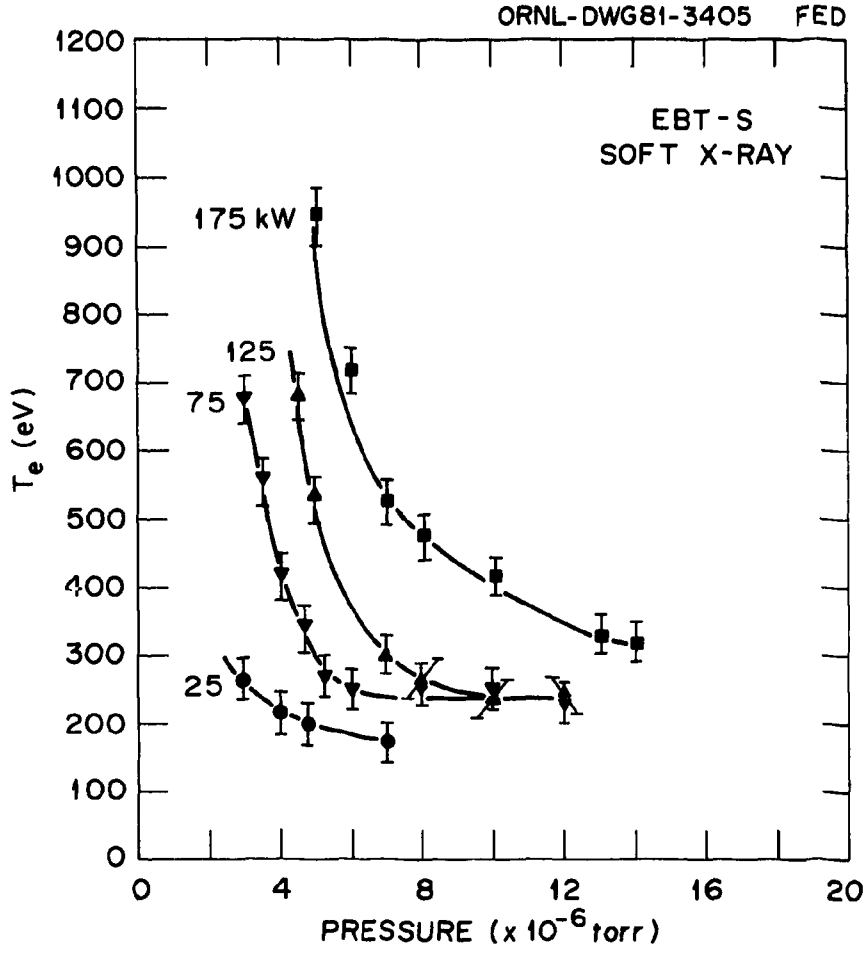
ORNL-DWG81-3405 FED
EBT-S
SOFT X-RAY
175 kW
125
75
25
T_e (eV)
1200
1100
1000
900
800
700
600
500
400
300
200
100
0
0
4
8
12
16
20
PRESSURE (x 10^{-6} torr)

Fig. 6

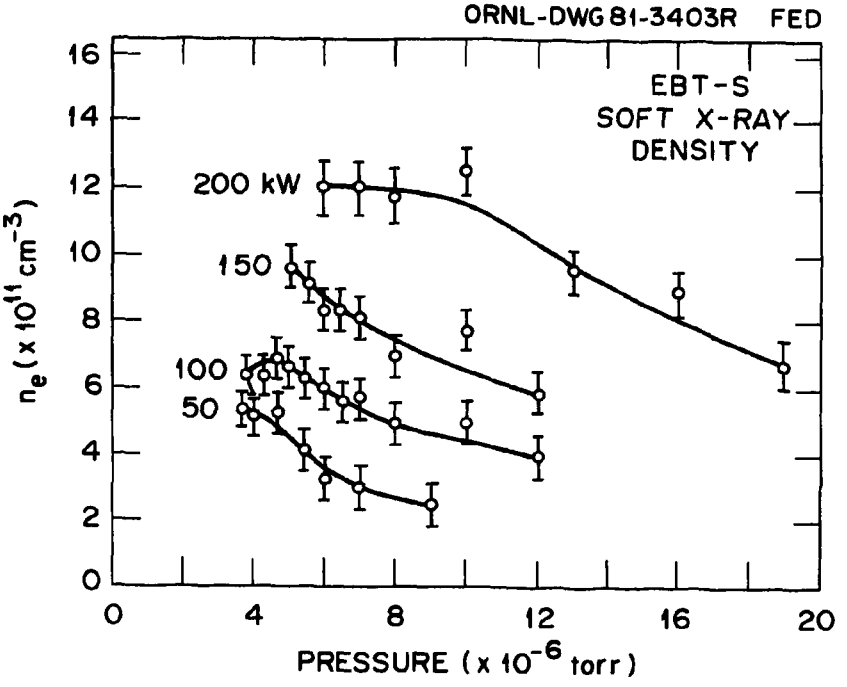
ORNL-DWG 81-3403R FED
EBT-S
SOFT X-RAY
DENSITY
200 kW
150
100
50
n_e (x 10^{11} cm^{-3})
PRESSURE (x 10^{-6} torr)
0
2
4
6
8
10
12
14
16
0
4
8
12
16
20

Fig. 7

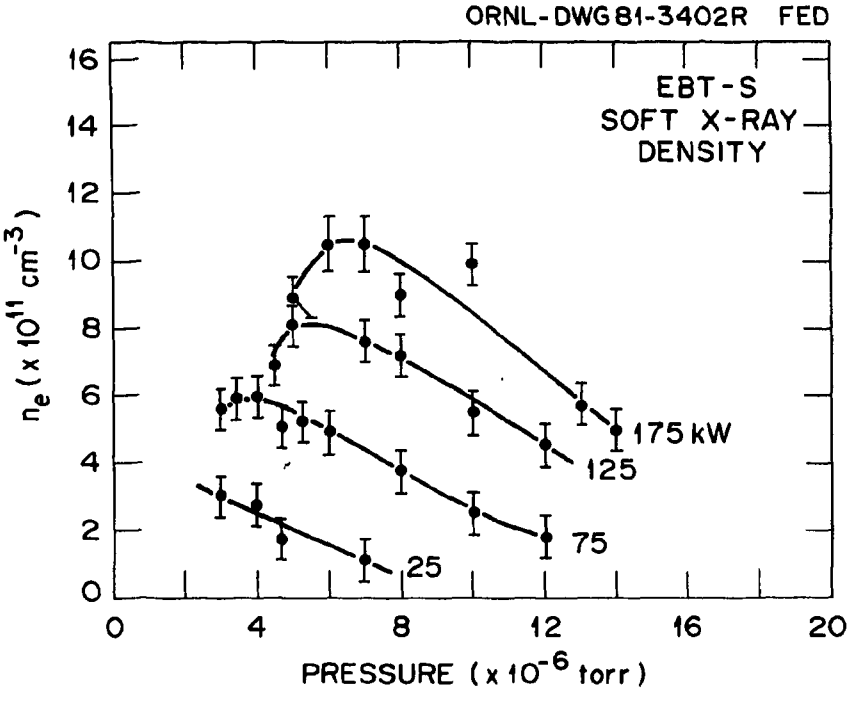
ORNL-DWG 81-3402R FED
EBT-S
SOFT X-RAY
DENSITY
n_e (x 10^{11} cm^{-3})
175 kW
125
75
25
PRESSURE (x 10^{-6} torr)
0
2
4
6
8
10
12
14
16
0
4
8
12
16
20

Fig. 8

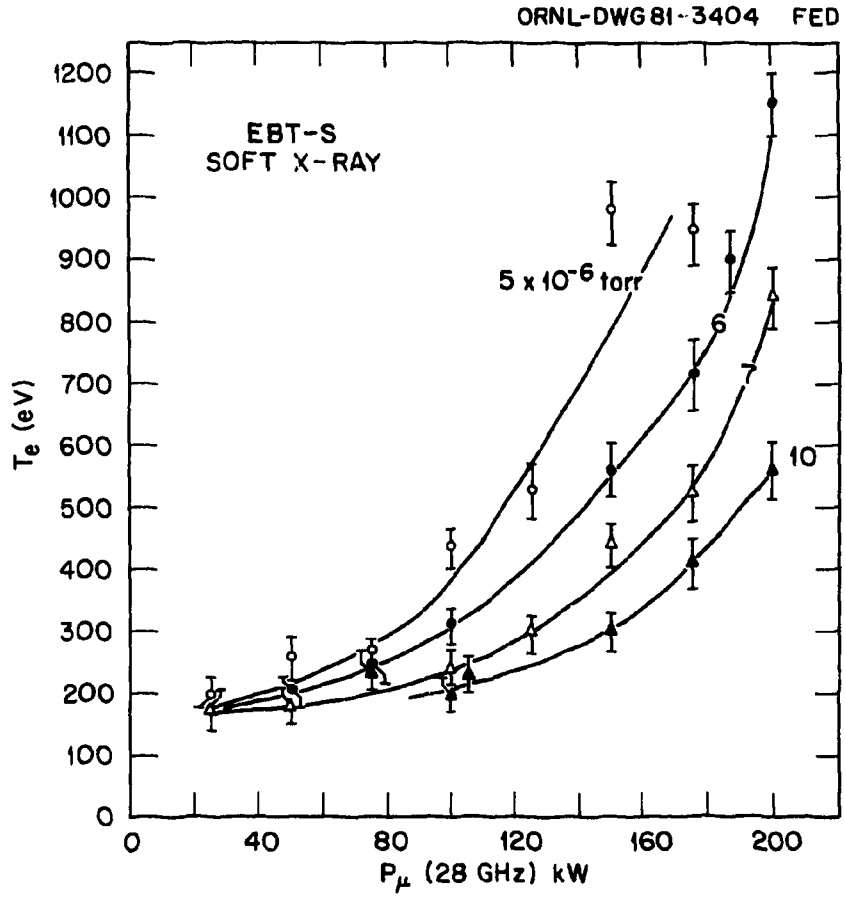
ORNL-DWG 81-3404 FED
EBT-S
SOFT X-RAY
5 x 10⁻⁶ torr
6
7
10
T_e (eV)
P_μ (28 GHz) kW
0
100
200
300
400
500
600
700
800
900
1000
1100
1200
0
40
80
120
160
200

Fig. 9

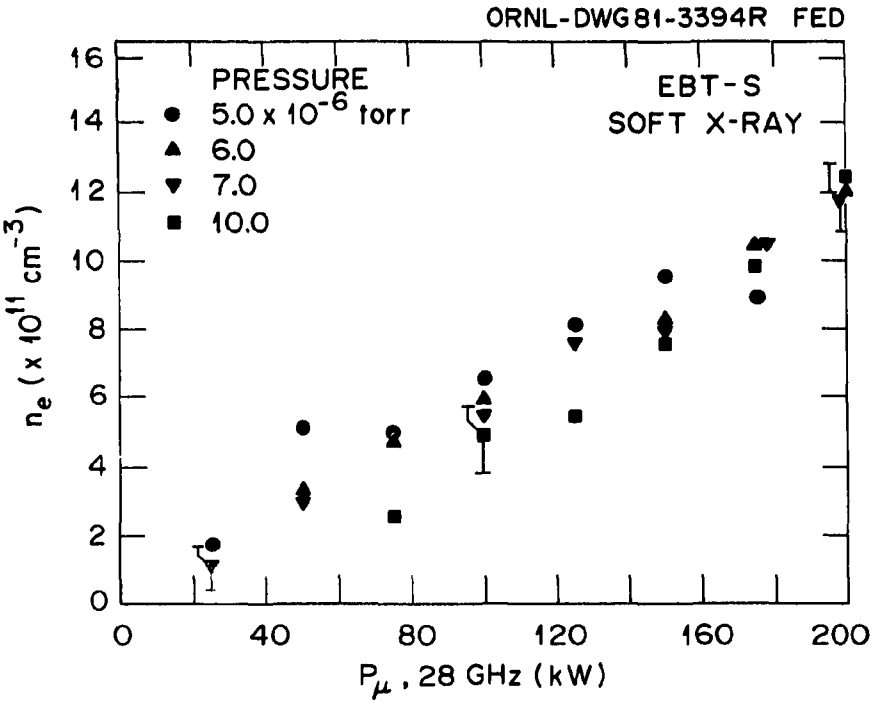
ORNL-DWG 81-3394R FED
PRESSURE
5.0 x 10^-6 torr
6.0
7.0
10.0
EBT-S
SOFT X-RAY
n_e (x 10^11 cm^-3)
P_μ, 28 GHz (kW)
0
2
4
6
8
10
12
14
16
0
40
80
120
160
200

Fig. 10

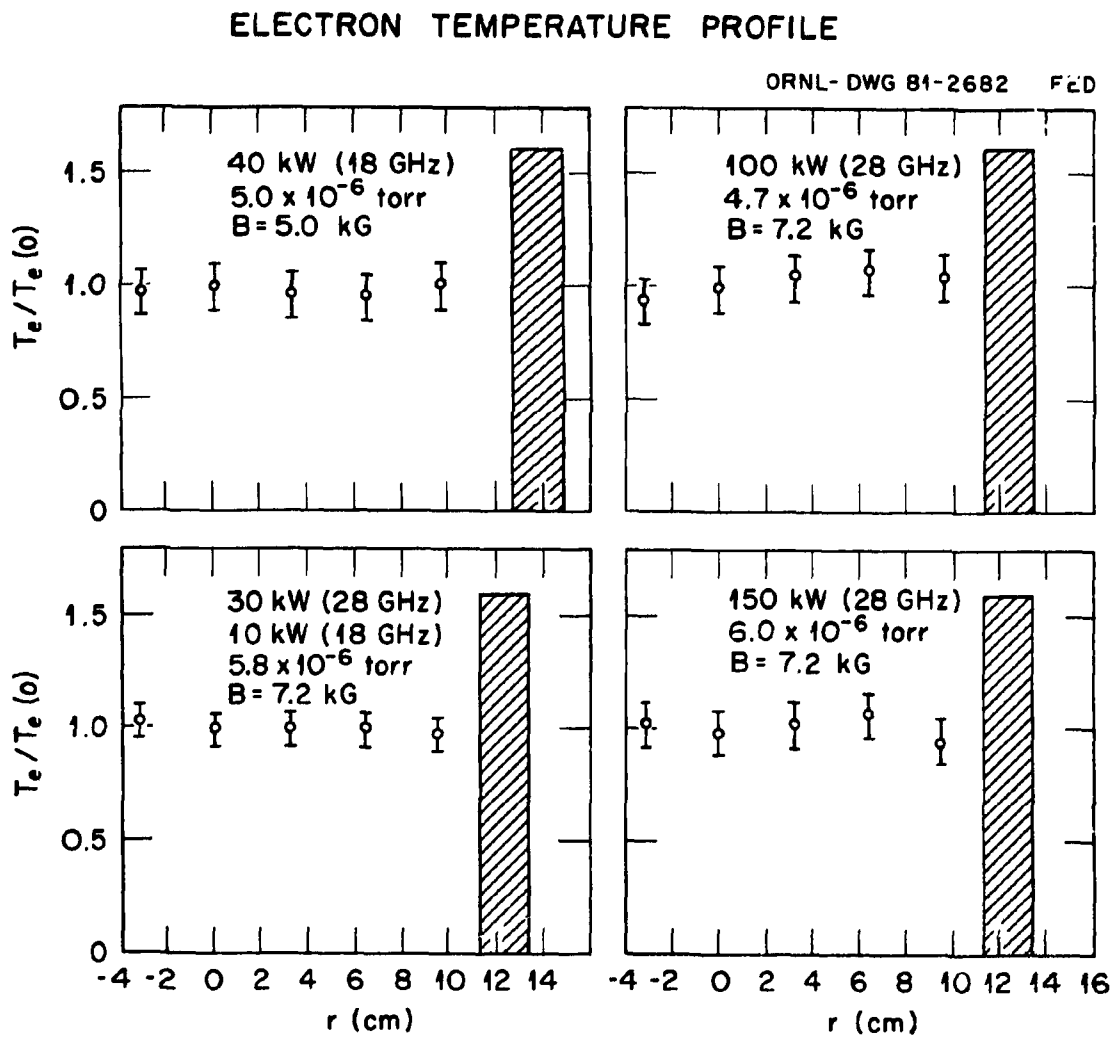
ELECTRON TEMPERATURE PROFILE
ORNL-DWG 81-2682 FED
40 kW (18 GHz)
5.0 x 10^-6 torr
B = 5.0 kG
100 kW (28 GHz)
4.7 x 10^-6 torr
B = 7.2 kG
30 kW (28 GHz)
10 kW (18 GHz)
5.8 x 10^-6 torr
B = 7.2 kG
150 kW (28 GHz)
6.0 x 10^-6 torr
B = 7.2 kG
Te/Te (o)
1.5
1.0
0.5
0
-4 -2 0 2 4 6 8 10 12 14
-4 -2 0 2 4 6 8 10 12 14 16
r (cm)

Fig. 11

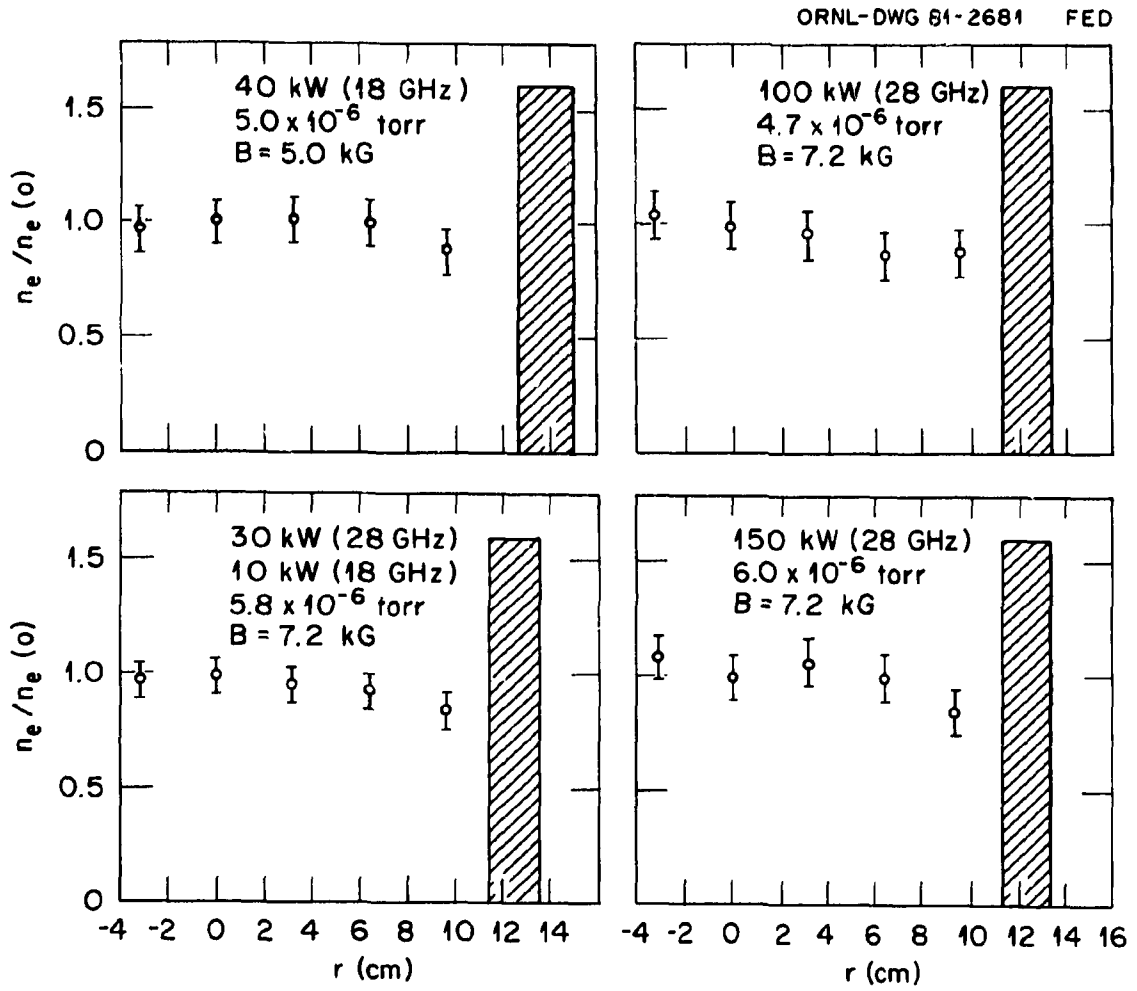
ELECTRON DENSITY PROFILES
ORNL-DWG 81-2681 FED
40 kW (18 GHz)
5.0 x 10^-6 torr
B = 5.0 kG
100 kW (28 GHz)
4.7 x 10^-6 torr
B = 7.2 kG
30 kW (28 GHz)
10 kW (18 GHz)
5.8 x 10^-6 torr
B = 7.2 kG
150 kW (28 GHz)
6.0 x 10^-6 torr
B = 7.2 kG
n_e / n_e (o)
1.5
1.0
0.5
0
-4 -2 0 2 4 6 8 10 12 14
-4 -2 0 2 4 6 8 10 12 14 16
r (cm)

Fig. 12

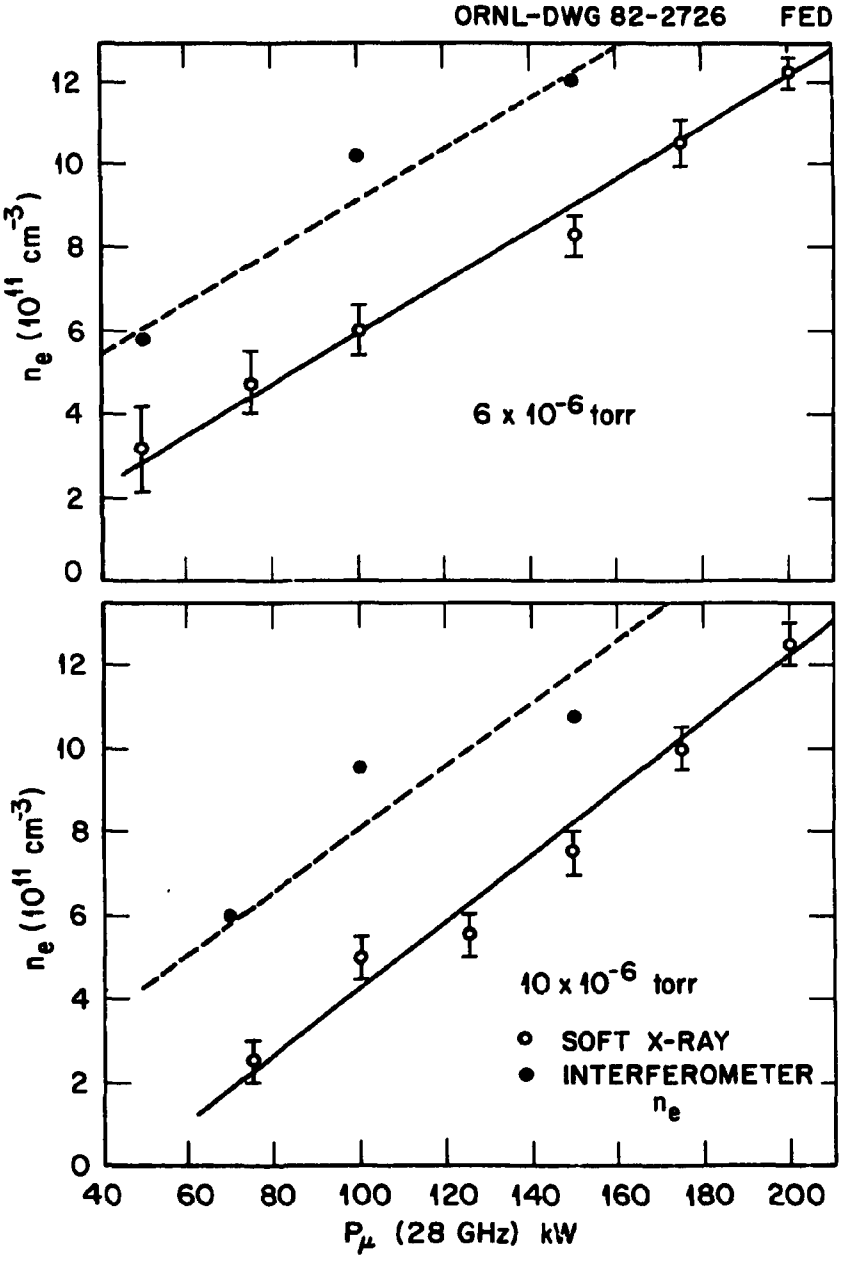
ORNL-DWG 82-2726 FED
n_e (10^{11} cm^{-3})
6 x 10^{-6} torr
10 x 10^{-6} torr
SOFT X-RAY
INTERFEROMETER n_e
P_μ (28 GHz) kW

Fig. 13

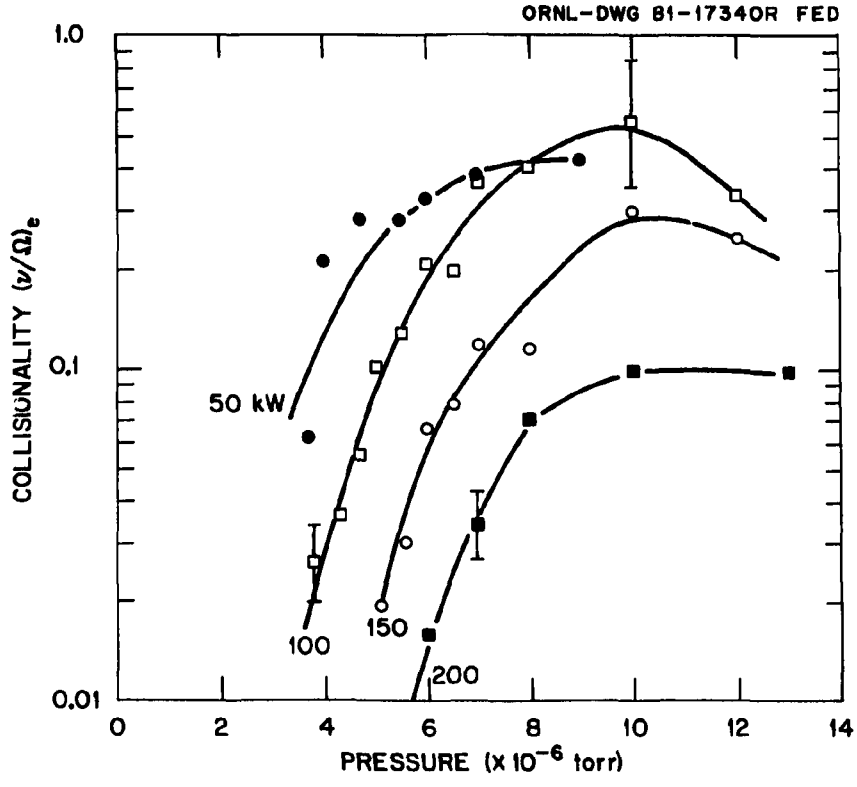
ORNL-DWG 81-17340R FED
1.0
0.1
0.01
COLLISIONALITY (ν/Ω)$_e$
50 kW
100
150
200
0
2
4
6
8
10
12
14
PRESSURE (x 10^{-6} torr)

Fig. 14

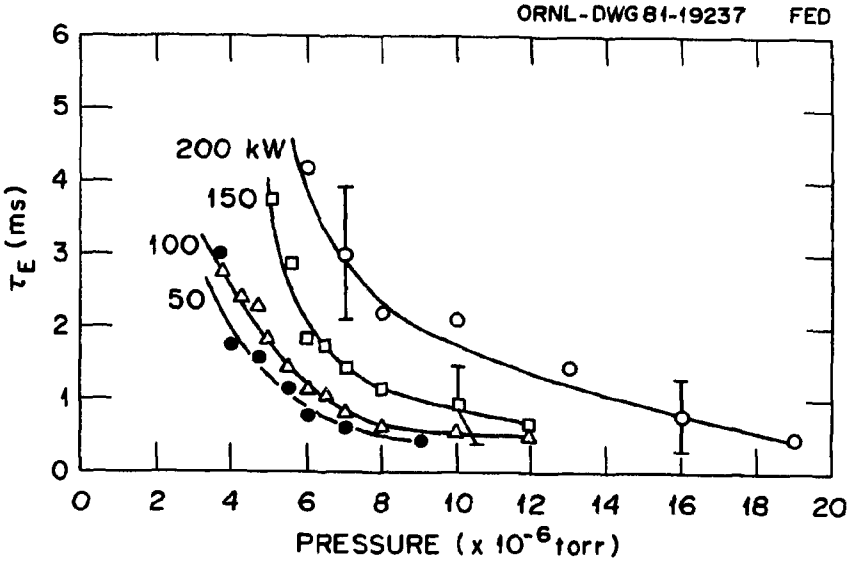
ORNL-DWG 81-19237 FED
200 kW
150
100
50
τ_E (ms)
PRESSURE (x 10^{-6} torr)
0
1
2
3
4
5
6
0
2
4
6
8
10
12
14
16
18
20

Fig. 15

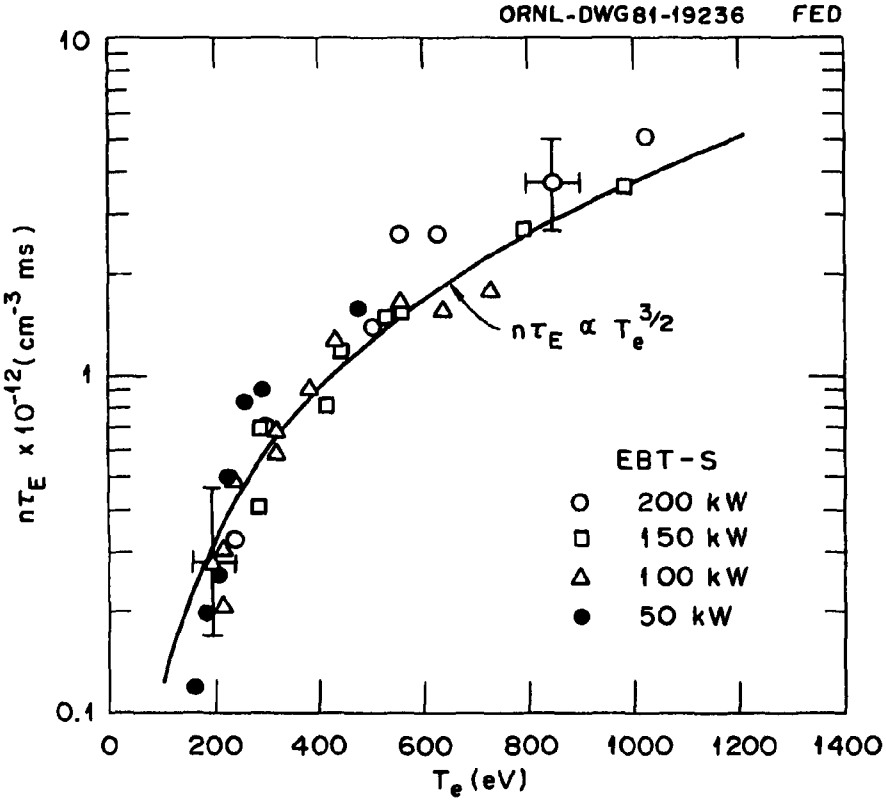
ORNL-DWG81-19236 FED
10
1
0.1
$n\tau_E$ x 10^{-12} (cm^{-3} ms)
0
200
400
600
800
1000
1200
1400
T_e (eV)
$n\tau_E \propto T_e^{3/2}$
EBT-S
200 kW
150 kW
100 kW
50 kW

Fig. 16

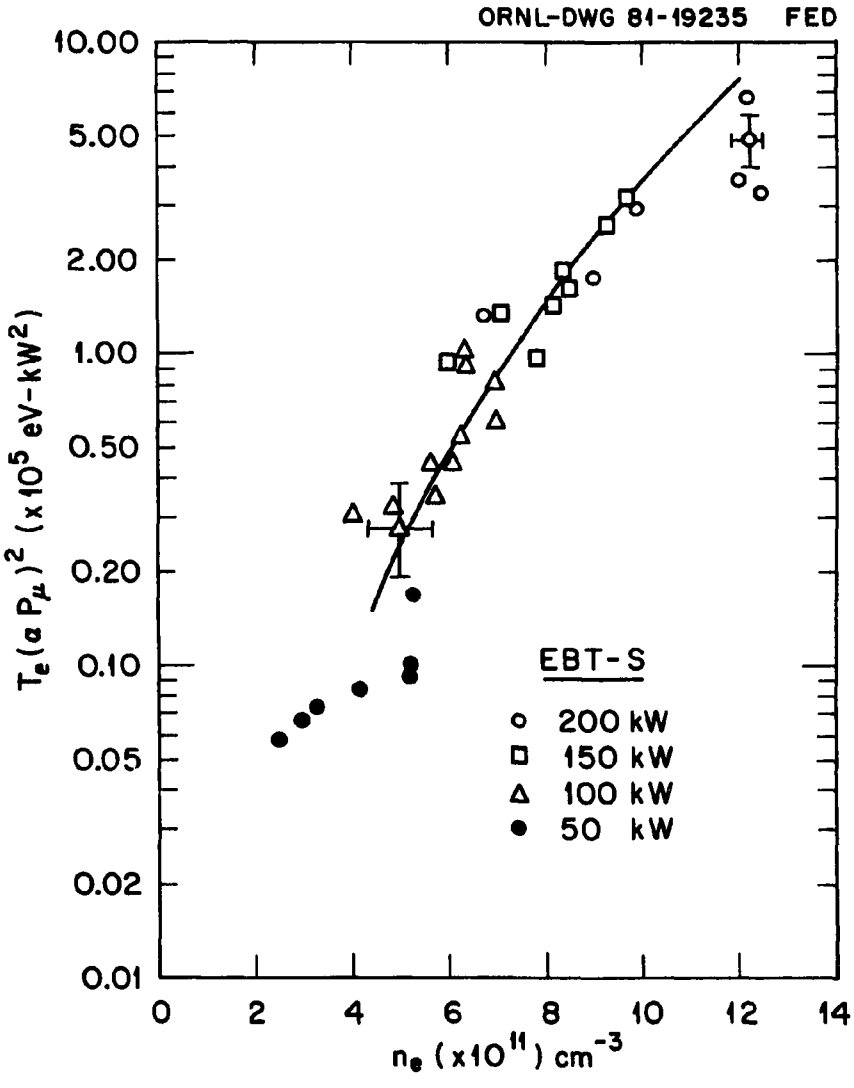
ORNL-DWG 81-19235 FED
10.00
5.00
2.00
1.00
0.50
0.20
0.10
0.05
0.02
0.01
$T_e(\alpha P_\mu)^2$ ($\times 10^5$ eV-kW^2)
0
2
4
6
8
10
12
14
n_e ($\times 10^{11}$) cm^{-3}
EBT-S
200 kW
150 kW
100 kW
50 kW

Fig. 17

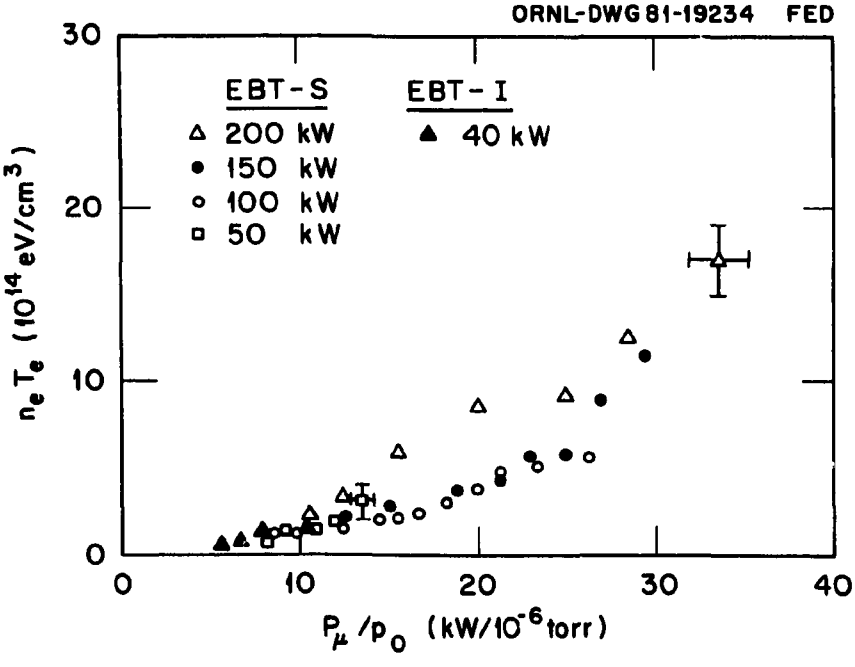
ORNL-DWG 81-19234 FED
EBT-S
EBT-I
200 kW
150 kW
100 kW
50 kW
40 kW
$n_e T_e$ (10^{14} eV/cm^3)
P_μ / p_0 (kW/10^{-6} torr)
0
10
20
30
40

Fig. 18